CONCRETE LIBRARY OF JSCE NO. 31, JUNE 1998

MODELING OF TENSILE AND SHEAR MECHANICAL PROPERTIES OF STEEL FIBER REINFORCED CONCRETE

(From Concrete Research and Technology, Vol.8, No.1, 1997)

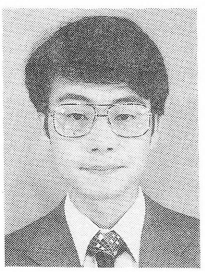

Tatsuya TSUBAKI

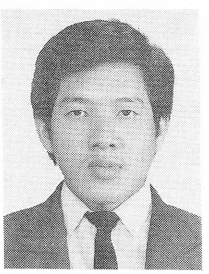

Sunaryo SUMITRO

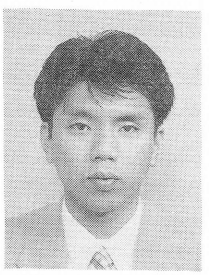

Hiroomi SHOJI

The mechanical properties of steel fiber reinforced concrete under tension and shear are investigated experimentally and mathematical models for the behavior are presented. High-strength concrete is used. The angle between a fiber and the crack surface is considered as a main parameter. The tensile behavior is influenced by the fiber angle, and the maximum load is reduced when the fiber is not perpendicular to the crack surface. Under shear loading, the maximum load is also reduced when the fiber angle is opposite to the shear direction. These experimental results are investigated by using a multi-linear material model and a parallel structural model simultaneously. The validity of the modeling is confirmed through simulation.

Keywords: *steel fiber reinforced concrete, tension, shear, mechanical properties, modeling*

Tatsuya Tsubaki is a Professor in the Department of Civil Engineering at Yokohama National University. He obtained his Ph.D. from Northwestern University in 1980. His research interests include the time-dependent mechanical behavior of concrete and the analysis of concrete structures. He is a member of the JSCE and the JCI.

Sunaryo Sumitro is a design engineer at Japan Structural Engineering and Computer Corporation in Tokyo. He is a former graduate student at Yokohama National University. He obtained his D.Eng. from Yokohama National University in 1997. His interests are related to the analysis and design of concrete structures. He is a member of the JSCE and the JCI.

Hiroomi Shoji is a construction engineer at Japan Highway Public Corporation. He is a former graduate student at Yokohama National University. He obtained his M.Eng. from Yokohama National University in 1996. His interests are mainly oriented to the construction of concrete bridge structures. He is a member of the JSCE and the JCI.

---

1. INTRODUCTION

Steel Fiber Reinforced Concrete (SFRC) can be considered a high-performance concrete with improved brittle properties. As such, it might be suitable for high-performance concrete structures, where it is essential for concrete to have high strength and high toughness. It has been noted that the tensile properties of concrete are improved effectively when steel fiber reinforcement is used, but there are still many uncertainties regarding the reinforcing mechanism in such concrete. For SFRC to become a practical material for use in concrete structures, it is essential to understand its deformational properties and clarify its reinforcing mechanism.

A constitutive equation is essential to the analysis of the behavior of an SFRC structure. A microstructure model has been proposed[1], but to make the model more sophisticated it is important to understand the behavior of SFRC under various loading conditions.

Regarding the tensile properties of SFRC, double tension experiment results have already been reported[2,3]. On the influence of fiber orientation, results for the behavior under tensile loading have been reported[4,5,6]. On shear behavior, the results of push-off shear tests on SFRC with stirrups have been reported[7]. However, there has been little research on deformational behavior under tension and shear using the same type of steel fiber. Therefore, in this research, the tensile and shear properties of SFRC are investigated experimentally with the parameters of fiber orientation, fiber spacing, and strength of the matrix. Furthermore, the modeling of the mechanical properties is also carried out. The behavior of SFRC after cracking is considered; behavior under uniaxial tension or shear is experimentally investigated using a specimen with a discontinuous surface simulating a crack. In relation to modeling the deformational properties, a microstructural analysis of bonding fractures around fibers has been reported[8]. Based on these experimental results, here a multi-linear material model is derived, and the appropriateness of the model is confirmed by implementing a simulation.

2. EXPERIMENTS ON SFRC

2.1 Uniaxial Tension Test

(1) Purpose

Under uniaxial tension, SFRC can sustain tension after full cracking as a result of the bridging effect of the steel fibers, as shown in Fig.1. It is necessary to understand the deformational behavior of steel fibers after full cracking in order to control cracking of the concrete. Therefore, in this study, specimens are artificially made with a discontinous plane as a crack plane, and the behavior of steel fibers in this plane due to tensile force is examined.

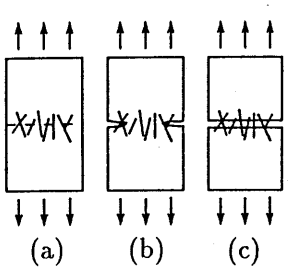

Fig.1 SFRC under Uniaxial Tension

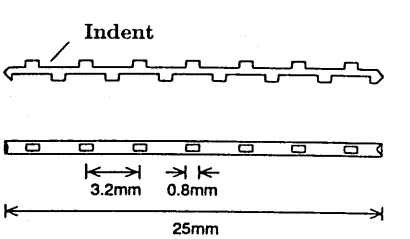

Fig.2 Geometry of Steel Fiber

(2) Materials

The materials used are shown in Table 1. These are ordinary Portland cement, river fine aggregate with a maximum size of 5mm, and straight-cut steel wire fibers with an indented surface. The geometry of the steel fibers is shown in Fig.2. In order to achieve a homogeneous matrix in the specimens, no coarse aggregate is used, and the matrix is mortar.

(3) Specimen and mix proportions

The shape and size of specimens for the uniaxial tension test are shown in Fig.3. A specimen consists of an upper block and a lower block. The discontinuous plane between these blocks is considered the crack plane. The size of the discontinuous plane is 100×100mm. Steel fibers are set to have a certain orientation to the discontinuous plane with the same embedment length in the two blocks. Here, the embedment length is the distance between the discontinuous plane and the fiber end measured along the fiber axis. The number of fibers is 32 (8 rows and 4 columns). Fibers are placed in a grid with a long side of 20mm and a short side of 10mm. Two fiber orientations, $\theta = 0°$ and $\theta = 45°$, were tested, where θ is the fiber orientation to the normal to the discontinuous plane. Figure 4 shows the configuration of the steel fibers in the central part of the specimen including the discontinuous plane. To achieve a symmetrical deformation during loading in the case of the 45° fibers, the fibers are arranged with opposite angles in alternating rows. Placing of the steel fibers in the specified position in the discontinuous plane was achieved by first embedding them in a styrofoam block. The upper specimen block was cast first in a metal form, and then the lower block was cast a day later. The specimen was cured in humid conditions, demolded at the age of 2 days, and stored under standard curing conditions (in 20°C water) up to the age of 28 days. Furthermore, to remove the bond at the discontinuous plane, two vinyl sheets were inserted at the time of casting.

The mix proportions of the mortar are shown in Table 2. The water-cement ratio (W/C) is 30% to obtain high-strength concrete. Mixing is by an Omni mixer. The mixing time is 4min. The number of specimens is three for each specimen type listed in Table 2.

(4) Loading method

Compressive force was applied directly to the lower part of the loading frame in a hydraulic universal testing machine. It was controlled by a load cell placed below the lower block of the specimen, as shown in Fig.5. The loading rate up to the peak was set to 0.25N for each fiber. This is about one third of the value in the JCI Standards[10] and was chosen to prevent sudden deformation. The pullout slippage of the fibers was measured with displacement transducers (LVDT) fitted to each side of the specimen.

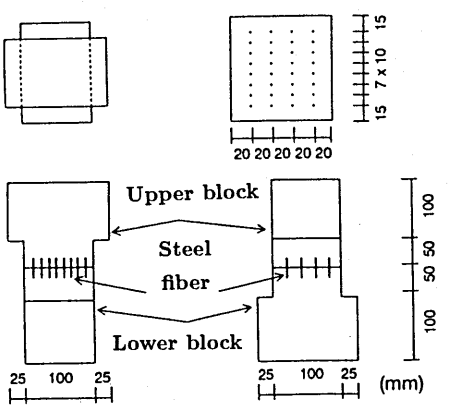

Fig.3 Specimens for Uniaxial Tension Test

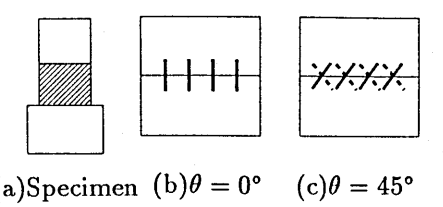

Fig.4 Steel Fiber Orientation in Specimens for Uniaxial Tension

Table 1 Materials Used in Experiment

Material	Description	
Water	Tap water (20°C)	
Cement	Ordinary Portland cement	(S.G.:3.16)
Fine Aggregate	River sand	(S.S.G.:2.46, F.M.:2.28)
Additive	Superplasticizer	Anion type agent
Steel Fiber	$\phi = 0.55$ (equivalent diameter), length 25mm, cut wire, indented surface, tensile strength 980N/mm^2	

[Note] S.G.: Specific gravity; S.S.G.: Surface-dry specific gravity; F.M.: Fineness modulus

Table 2 Test Specimens and Mix Proportions

Test	Specimen[1)]	Fiber Arrangement			W/C (%)	S/C	Unit Amount[3)] (kg/m^3)		
		Number of Fibers[2)]	Spacing (mm)	Angle (deg)			W	C	S
Uniaxial Tension	TH–32–0	32	20,10	0	30	1.0	292	974	974
	TH–32–45			45					
Shear	SH–64–0	64	10	0	30	1.0	292	974	974
	SH–64–45	64	10	−45					
	SH–64+45	64	10	+45					
	SH–256–0	256	5	0					
	SN–64–0	64	10	0	50	2.0	305	610	1220

[Note] 1) Specimen type: [T(uniaxial tension), S(shear)][H(high strength), N(normal strength)]–[No. of fibers]–[Angle θ (see Figs.7,12,13)]
2) For shear, represents the number of fibers in one shear plane.
3) W(water), C(cement), S(sand)

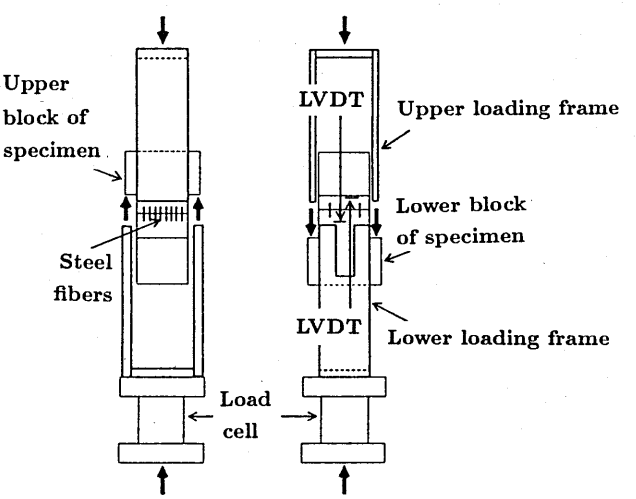

Fig.5 Loading Method for Uniaxial Tension Test

2.2 Shear Test

(1) Porpose

Fibers in the shear plane of SFRC are in general randomly distributed (see Fig.6(a,b)). The shear force, after forming a shear plane, is sustained by the shear transfer mechanism of the fibers together with friction and aggregate interlock. To investigate the basic deformational properties of steel fibers under shear loading, specimens in which steel fibers are arranged on the square grid points at a specified orientation and with the same embedment length on each side of a pre-placed discontinuous plane (shear plane) are prepared (see Fig.6(c)).

(2) Materials

The mortar materials and steel fibers used in the shear test are the same as those for the uniaxial test (see Table 1 and Fig.1).

(3) Specimen and mix proportions

The size of the specimen is $100 \times 100 \times 400$mm. All specimens are shown in Fig.7 and summarized in Table 2. A specimen was loaded along two shear planes (see Fig.8). There are two types of specimens as regards number of fibers and spacing, i.e., 64 (8×8) fibers with 10mm spacing and 256 (16×16) fibers with 5mm spacing. Three fiber orientations were tested: $\theta = 0°$, $\theta = +45°$, and $\theta = -45°$, where θ is the fiber orientation to the horizontal axis (see Fig.7). Concerning mortar strength, high-strength mortar with W/C=30% and normal-strength mortar with W/C=50% were used. To allow the position of steel fibers in the shear plane to be fixed, the right and left parts of the specimen were cast the day after the middle part. All specimens were cured under humid conditions, demolded at the age of 2 days, and stored under standard curing conditions (in 20°C water) until the age of 28 days. To avoid bonding at the shear plane, two vinyl sheets were inserted at each plane at the time of casting. The mixing time for mortar and the number of specimens for each specimen type are the same as for the uniaxial tension test.

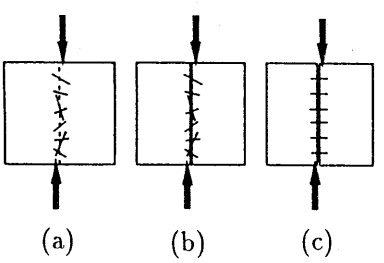

Fig.6 SFRC under Shear

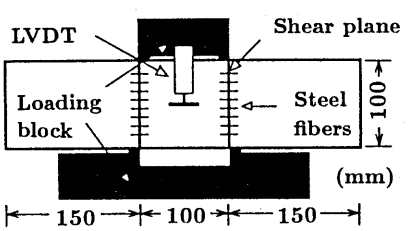

Fig.8 Loading Method for Shear Test

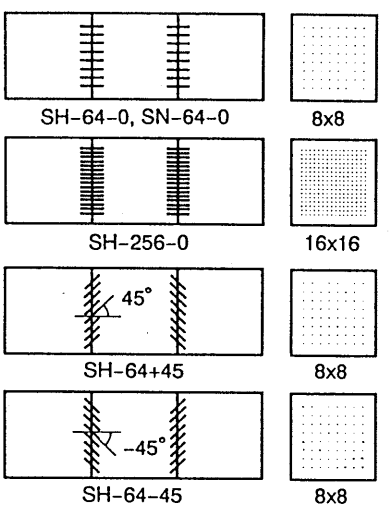

Fig.7 Specimens for Shear Test

(4) Test method
The shear test was based on the shear strength test procedure for SFRC[10]. The test apparatus is shown in Fig.8. The load was applied by a hydraulic universal testing machine. The loading rate was the same as in the uniaxial tension test. The shear displacement from the base plane was measured at the center of a specimen by two LVDTs placed at the symmetric positions.

3. EXPERIMENTAL RESULTS

3.1 Results of Tests on Material Properties

The compressive strength of the mortar was obtained from tests of cylindrical specimens measuring 50mm in diameter and 100mm in height. The average values are 54.0N/mm^2 for the high-strength mortar and 32.1N/mm^2 for the normal-strength mortar.

3.2 Results of Uniaxial Tension Test

The tension-axial displacement relationship under uniaxial tension is shown in Fig.9. The tension is the total tension load while the displacement is the average value of relative displacement at the discontinuous plane measured on both sides of the specimen. The maximum load for the $\theta = 45°$ case is less than the $\theta = 0°$ case by a factor of 26%. The displacement at maximum load is almost the same (about 1mm) in both cases. Nonlinear behavior up to maximum load and softening behavior after maximum load are observed. The bond strength of each fiber, calculated by dividing the maximum load by the number of fibers, is 138N for the $\theta = 0°$ case and 102N for the $\theta = 45°$ case. The failure conditions of test specimens are shown in Table 3. All fibers are pulled out at failure, so all specimens can be classified as suffering pullout failure. The pullout holes, where the mortar failed, around the fiber for the $\theta = 45°$ case are larger than for the $\theta = 0°$ case; in fact, the mortar failure region sometimes extends to the adjacent two or three fibers. It is deduced that local mortar failure around a fiber causes a reduction in tensile stiffness and tensile strength.

3.3 Results of Shear Test

The average shear load-shear displacement relationships for one shear plane obtained from specimens with two shear planes (on the left and right sides) are shown in Figs.10 and 11, while the conditions of failure are described in Table 3.

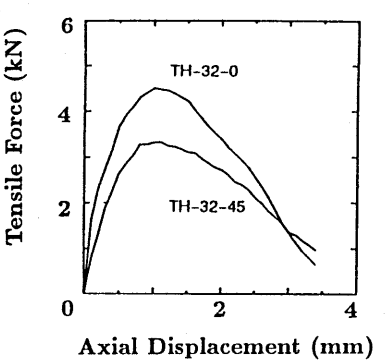

Fig.9 Tensile Force–Displacement Relationship for Uniaxial Tension

Table 3 Failure Conditions of Test Specimens

Test	Specimen	Failure Condition[1] of Steel Fiber				Mortar Failure[2] around Fiber
		Pullout (%)	Pullout Rupture(%)	Rupture (%)	Type	
Uniaxial Tension	TH–32–0	100	0	0	Pullout	Small
	TH–32–45	100	0	0	Pullout	Large
Shear	SH–64–0	50	47	3	Mixed	Small
	SH–64–45	86	12	2	Pullout	Large
	SH–64+45	27	70	3	Mixed	Large
	SH–256–0	6	79	15	Rupture	Small
	SN–64–0	100	0	0	Pullout	Large

[Note] 1) Rupture: for $l_{rup} < 1$mm; pullout rupture: for 1mm $\leq l_{rup} \leq$ 5mm; pullout: for $l_{rup} >$ 5mm where l_{rup} is the pullout length of the fiber at rupture or at the end of loading.

2) Small: for $\phi_{ave} \leq$ 5mm; large: for $\phi_{ave} >$ 5mm where ϕ_{ave} is the average of the longer diameter of the elliptic mortar failure zone around the fiber as projected onto the discontinuous (crack) plane.

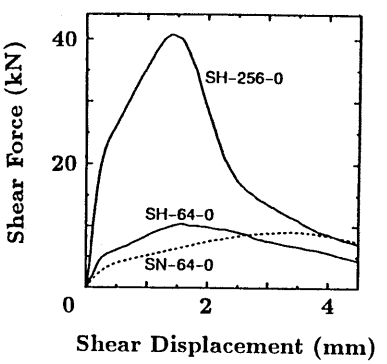

Fig.10 Shear Force–Displacement Relationship (Effect of Mortar Strength, Number of Fibers, and their Spacing)

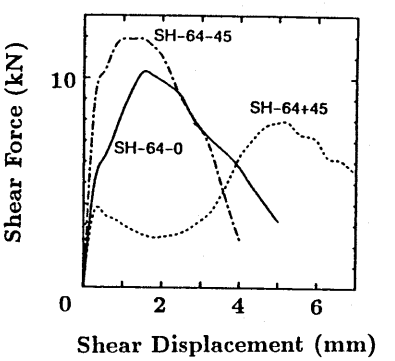

Fig.11 Shear Force–Displacement Relationship (Effect of Fiber Orientation)

Figure 10 indicates the effects of mortar strength, number of fibers, and fiber spacing. For each specimen, there is softening behavior after the peak load is reached. Comparing specimens SH–64–0 and SN–64–0, it is noteworthy that their peak shear forces are about the same but they occur at different displacements. In the high-strength mortar case, the shear force reaches a maximum when the displacement is 1.5mm, while for normal-strength mortar case, this occurs at a displacement of 3.5mm. All steel fibers are pulled out in failure for specimen SN–64–0. But with specimen SH–64–0, fiber failures can be classified as pullout failure (50%), pullout rupture failure (47%), and rupture failure (3%). This classification of failure conditions is made by observing the rupture length (pullout length of fiber at failure) of steel fibers in the shear plane after loading. A rupture failure is defined as a rupture length of less than 1mm, a pullout rupture failure as a rupture length of more than

1mm, and a pullout failure as a rupture length greater than 5mm. The definition of pullout failure is determined by the capacity of the LVDT (5mm). It is found that debonding propagates at an early stage in specimen SN–64–0, where pullout failure occurred. Thus, this specimen was more ductile and less stiff than specimen SH–64–0 which underwent mixed (pullout and rupture) failure. It is also clear that the deformational behavior of specimen SN–64–0 is influenced by the large failure zone around a fiber pullout hole in the mortar.

For the high-strength specimen SH–256–0, the ratios of pullout failures, pullout rupture failures, and rupture failures are 6%, 79%, and 15%, respectively. Almost all fibers show same degree of rupture failure. This is because the fiber spacing is one half that of specimen SH–64–0. The maximum shear force on one fiber calculated by dividing the total maximum load by the number of fibers is about the same as that of SH–64–0 (157N). The shear displacement at the maximum load is also identical (1.5mm). However, the softening behavior of specimen SH–256–0, where rupture failure occurred, indicates more brittle characteristics.

Figure 11 shows the effect of fiber orientation. The shear force in the case of specimen SH–64–45, where fibers are angled at 45° toward the shear force direction, is larger than that in the case of specimen SH–64–0, while shear displacement at the maximum load is slightly smaller. This is because 86% of the fibers suffer pullout failure and the failure zone of mortar around the fibers is large. On the other hand, the load for specimen SH–64+45, where fibers are angled at 45° in the opposite direction to the shear force, decreases initially, then keeps rising to reach the maximum load until eventually strain softening occurs after the peak load. Compared to specimens SH–64–0 and SH–64–45, the maximum load is smaller and the shear displacement at the peak is about three times larger. It is deduced that the initial reduction in load is caused by local failure of the mortar around the fibers and local bending of fibers. The ratio of pullout failure fibers is 27%. As a result of fiber orientation, a high percentage of rupture failures is observed. Consequently, this type of failure is classified as mixed.

Mortar failure around fibers is observed mainly where either pullout failure or pullout rupture failure occurred. Based on the size of the approximately elliptic area obtained by projecting the mortar failure zone onto the discontinuous plane, these mortar failures are classified as 'large' if the average of the length of the longer axis is more than 5mm and 'small' if it is less than 5mm. The total area of the mortar failure zone is estimated from the product of the average size of a mortar failure and the number of fibers suffering pullout failure.

Because of short embedment length and small diameter of fibers, the shear capacity of steel fibers is much smaller than that of ordinary reinforcing bars. In addition, there are still uncertain points in the deformational characteristics of SFRC under shear because of insufficient research investigation. Therefore, the shear capacity of steel fibers is neglected in the design of SFRC. In this study, fibers are embedded by the same amount on both sides of the shear plane to ensure most effective resistance to shear loading. Nevertheless, from these experimental results, it is confirmed that in some cases, the contribution of shear stiffness and shear strength cannot be neglected.

4. MODELING OF DEFORMATIONAL BEHAVIOR OF SFRC

The deformational behavior of SFRC under uniaxial tension and shear is modeled as shown in Figs.12 and 13. The primary influences considered are debonding, local mortar failure due to fiber orientation, and tensile rupture of fibers.

The deformational behavior for SFRC under uniaxial tension (model T-1) is given in Fig.14. After full cracking, the tensile properties of SFRC are influenced by various factors such as concrete strength, fiber type, fiber angle, and fiber volume fraction[2]. Global behavior is assumed to be governed by the

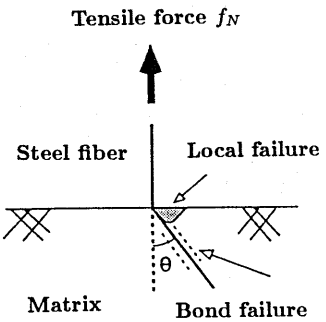

Fig.12 Failure Condition of Steel Fiber under Uniaxial Tension

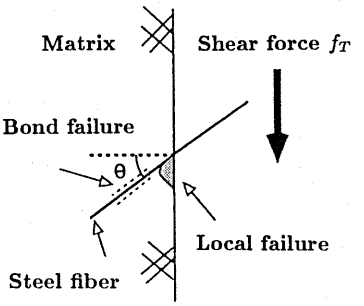

Fig.13 Failure Condition of Steel Fiber under Shear

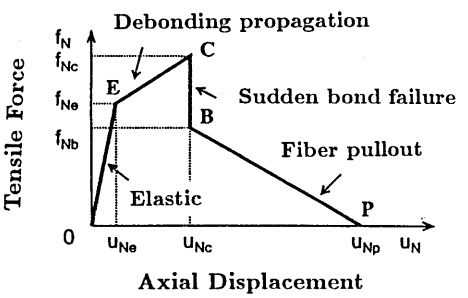

Fig.14 Bond Force–Displacement Relationship under Uniaxial Tension (Model T–1)

relationship between bond failure and pullout of steel fibers from mortar, as shown in Fig.14. This relationship is expressed by a multi-linear material model which is linear from the origin O to point E, where behavior is elastic because of the perfect bond between fiber and matrix. After reaching point E, the bond stiffness falls along EC because the debonding process starts at the discontinuum plane. Then, the bond force decreases suddenly to point B because of total bond failure. After sudden failure, continuing pullout of the fibers takes place until point P. The influence of local mortar failure near the crack plane, which depends on fiber angle, is expressed by the gradient between point E and point C.

In the case of shear, it is assumed that local matrix failure occurs in the mortar below the steel fibers near the shear plane, and then either fiber rupture or fiber pullout occurs. Thus, for the relationship between mean shear force and shear displacement, a similar relationship to that used for uniaxial tension can be applied. The model for the deformational behavior under shear (model S-1) is shown in Fig.15. From the origin O to point E, the fibers behave elastically. After reaching point E, debonding starts, causing a stiffness reduction. Debonding continues up to the maximum sustainable load level at point C. The sustained load drops to zero in the case of fiber rupture, or suddenly decreases to point B due to bond failure and then falls to point P as successive fiber pullout proceeds until all fibers are pulled out.

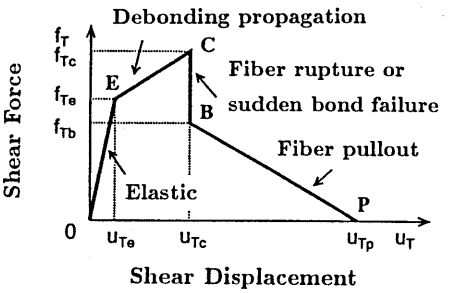

Fig.15 Bond Force–Displacement Relationship under Shear (Model S–1)

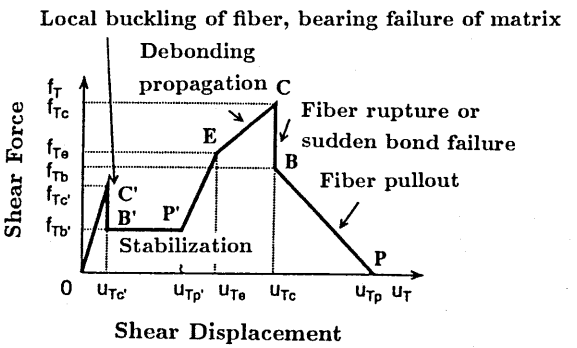

Fig.16 Bond Force–Displacement Relationship under Shear (Model S–2)

The deformational behavior of steel fibers angled opposite to the shear direction (model S-2) is shown in Fig.16. In this case, local mortar failure and local fiber bending at the early stage of point C' are followed by a stable state along B'P'. The subsequent behavior is modeled in the same way as model S-1.

By adopting the parallel structural model shown in Fig.17, the test results obtained in uniaxial tension and shear experiments are simulated numerically. This parallel structural model assumes that all fibers have the same spacing and are arranged normal to the discontinuous plane. The effects of fiber orientation are taken into account by adjusting the gradient up to the maximum load. All fibers are embedded in a rigid block, so the same displacement is applied to each fiber in either the axial or lateral direction. Non-uniformity in the material properties of the fibers and the bond zone is taken into account by applying a statistical variation (see Fig.18). The global behavior of one specimen is obtained by superimposing the deformational behavior of all fibers. In this simulation, the length of each fiber is kept constant (unity). The material constants, aside from m_t, n_t, m_s, n_s, are given a statistical variation consisting of a uniform distribution with a one-side scatter width ω of 30% of the mean (see Tables 4 and 5). The variation of all material constants is the same for each fiber and the number of fibers is the same as the actual number of fibers for each test specimen. The simulation is based on the displacement increment method, with incremental small displacements applied to the rigid block in the parallel structural model. The analysis procedure is summarized as follows.

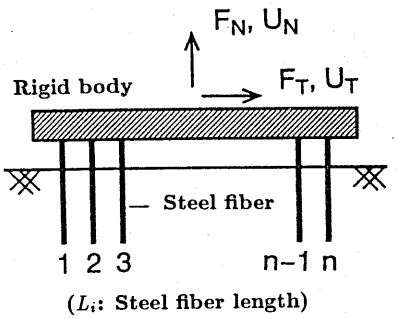

Fig.17 Parallel Structural Model

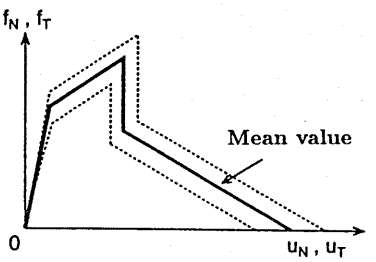

Fig.18 Statistical Variation of Material Constants

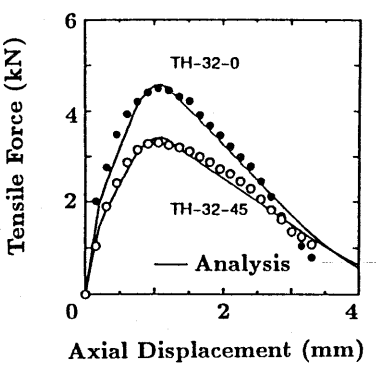

Fig.19 Simulation of Uniaxial Tension Behavior

1) Impose a small displacement increment, ΔU, on the rigid body in the parallel structural model to cause an equal displacement u to each fiber at the discontinuous plane.
2) Determine the stiffness of each fiber considering the statistical scatter of material constants at the current load step based on the load-displacement relationship shown in Figs.14, 15, and 16.
3) Calculate the force f acting on each fiber.
4) Calculate the total force F by summing up the force on each fiber.
5) Repeat the above steps up to the specified displacement.

In this procedure, the force on each fiber at the discontinuous plane f and its displacement u are expressed by f_N and u_N for uniaxial tension and f_T and u_T for shear. The total force and the mean displacement are expressed by F_N, F_T and U_N, U_T, respectively (see Fig.17). The optimum values of the material parameters are obtained by a trial-and-error approach, fitting the force-displacement curve corresponding to each test data.

The simulation results for uniaxial tension and shear are expressed by the solid lines in Figs.19, 20, and 21. A comparison with the test results confirms the applicability of this multi-linear material model.

The mean values of material parameters used in the simulation with this multi-linear material model are shown in Tables 4 and 5. The single fiber mechanical models for uniaxial tension and shear shown in Figs.14–16 are obtained from the test data. By adopting a mechanical model considering debonding propagation at the fiber-mortar interface as previously proposed by the authors[11], it is confirmed that the multi-linear material model can simulate well the deformational behavior of SFRC under uniaxial tension. Because the actual behavior is nonlinear, for given accuracy, the values of material constants might vary. Here, the mean values of material constants are determined by considering the variations in the test data.

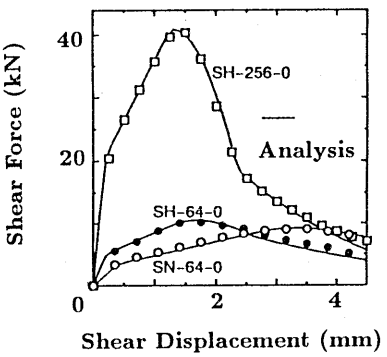

Fig.20 Simulation of Shear Behavior (Effect of Mortar Strength, Number of Fibers, and their Spacing)

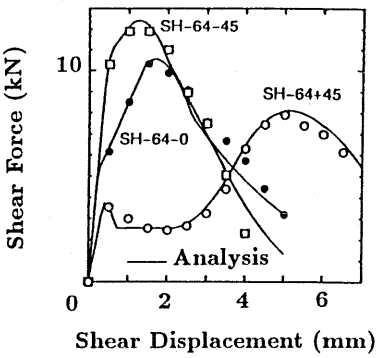

Fig.21 Simulation of Shear Behavior (Effect of Fiber Orientation)

Table 4 Material Constants Used in Uniaxial Tension Simulation

Specimen	f_{Nc} (N)	f_{Nb} (N)	m_t ($f_{Ne} = m_t f_{Nc}$)	u_{Nc} (mm)	u_{Np} (mm)	n_t ($u_{Ne} = n_t u_{Nc}$)	ω (%)
TH–32–0	157	147	0.4	1.0	4.1	0.1	30
TH–32–45	118	108	0.4	1.0	4.5	0.2	30

[Note] The definitions of tensile forces, f_{Nc}, f_{Nb}, and axial displacements, u_{Nc}, u_{Np} are given in Fig.14. m_t and n_t are constant ratios defining the elastic limit. ω is the one-side scatter width, which is common for all variables.

Table 5 Material Constants Used in Shear Simulation

Specimen	f_{Tc} (N)	f_{Tb} (N)	m_s ($f_{Te} = m_s f_{Tc}$)	u_{Tc} (mm)	u_{Tp} (mm)	n_s ($u_{Te} = n_s u_{Tc}$)	ω (%)
SH–64–0	196	157	0.4	2.0	10.0	0.1	30
SH–64–45	206	186	0.8	1.5	5.0	0.3	30
SH–64+45	176	147	0.5	5.5	12.0	0.4	30
SH–256–0	196	98	0.4	1.8	7.5	0.1	30
SN–64–0	176	147	0.3	4.0	10.0	0.1	30

[Note] The definitions of shear forces, f_{Tc}, f_{Tb}, and shear displacements, u_{Tc}, u_{Tp} are given in Fig.15. m_s and n_s are constant ratios defining the elastic limit. ω is the one-side scatter width, which is common for all variables. For specimen SH–64+45, $f'_{Tc} = 7.8$N, $f'_{Tb} = 3.9$N, $u'_{Tc} = 0.5$mm, $u'_{Tp} = 3.0$mm (see Fig.16).

5. CONCLUSIONS

The post-cracking deformational behavior of SFRC under uniaxial tension and shear has been investigated experimentally, with the effects of the number of fibers, the fiber spacing, the fiber angle, and the concrete strength taken into account. Furthermore, the deformational behavior is modeled. The appropriateness of the model is confirmed through simulations. The following is a summary of the study.

1) The mechanical properties of SFRC under uniaxial tension are influenced by the orientation of the steel fibers. The maximum load is reduced when the fibers are not perpendicular to the crack surface (θ=45°).
2) Under shear loading, the mechanical properties are influenced by the fiber spacing, their angle, and the strength of the matrix. The maximum load is reduced when the fibers are angled opposite the shear direction. With this fiber orientation, the shear behavior is different from other cases.
3) The deformational behavior of SFRC under uniaxial tension and shear can be expressed by both a multi-linear material model and a parallel structural model.

The mechanical properties of SFRC are also influenced by the effects of fiber type and matrix strength, and these will be clarified by extending the present study.

ACKNOWLEDGEMENT

The support provided to one of the authors by Grant-in-Aid for Scientific Research (C) from the Ministry of Education is gratefully acknowledged.

REFERENCES

(1) Sumitro, S. and Tsubaki, T., "Micromechanical Constitutive Relationship of Fiber Reinforced Concrete," Proc. of the JCI, Vol 18, No.2, pp.419–424, 1996
(2) Cho, R. and Kobayashi, K., "Testing Method for Tensile Strength of Steel Fiber Reinforced Concrete," Concrete Journal, JCI, Vol.17, No.9, pp.87–95, 1979
(3) Masuda, K., Uomoto, T., and Nishimura, T., "Tensile Properties of Steel Fiber Reinforced Concrete and Fiber Types," Proc. of 47th JSCE Annual Conf., V, No.121, pp.272–273, 1992
(4) Naaman, A.E. and Shah, S.P., "Pull-Out Mechanism in Steel Fiber-Reinforced Concrete," J. of Struct. Div., Proc. of ASCE, Vol.102, No.ST8, pp.1537–1548, 1976
(5) Li, V.C., Wang, Y., and Backer, S., "Effect of Inclining Angle, Bundling and Surface Treatment on Synthetic Fibre Pull-Out from a Cement Matrix," Composites, Vol.21, No.2, pp.132-140, 1990
(6) Ouyang, C., Pacios, A., and Shah, S.P., "Pullout of Inclined Fibers from Cementitious Matrix," J. of Engrg. Mech., ASCE, Vol.120, No.12, pp.2641–2659, 1994
(7) Valle, M. and Büyüköztürk, O., "Behavior of Fiber Reinforced High-Strength Concrete under Direct Shear," ACI Materials Journal, Vol.90, No.2, pp.122–133, 1993
(8) Stang, H., Li, Z., and Shah, S.P., "Pullout Problem: Stress versus Fracture Mechanical Approach," J. of Engrg. Mech., Vol.116, No.10, pp.2136–2150, 1990
(9) Shoji, H., Tsubaki, T., and Sumitro, S., "Deformational Properties of SFRC and Their Modeling," Proc. of the JCI, Vol 18, No.2, pp.1409–1414, 1996
(10) JCI,"JCI Standards for Test Methods of Fiber Reinforced Concrete," JCI-SF, pp.57–59, 65–68, 1984
(11) Sumitro, S. and Tsubaki, T., "Pullout Model for Steel Fiber Reinforced Concrete," Proc. of 51st JSCE Annual Conf., V, No.556, pp.1110–1111, 1996